Frontiers in Bioscience Landmark

Front. Biosci. (Landmark Ed) **2026**; 31(6): 48958
https://doi.org/10.31083/FBL48958

Original Research

Identification of the Mitochondrial Gene *NME6* as an Immune Modulator in Heart Failure

Pan Liu[1,2,†], Fan Yang[2,†], Yang Zhang[3], Jingjing Kong[2], Xianwei Qi[2], Liang Yuan[2], Jing Wang[1], Xiaoyu Qiang[4], Shiguang Wang[2,*], Ran Xia[1,*]

[1]Zhongyi School, Anhui University of Chinese Medicine, 230012 Hefei, Anhui, China
[2]Department of Cardiology, The First Affiliated Hospital of Anhui University of Chinese Medicine, 230013 Hefei, Anhui, China
[3]Department of Central Laboratory, The Third People's Hospital of Bengbu Affiliated to Bengbu Medical University (Bengbu Central Hospital), 233099 Bengbu, Anhui, China
[4]School of Basic Medicine Science, Shanghai University of Traditional Chinese Medicine, 201203 Shanghai, China
*Correspondence: dr_shguang@ahtcm.edu.cn (Shiguang Wang); ranranxia@ahtcm.edu.cn (Ran Xia)
[†]These authors contributed equally.
Academic Editors: Paramjit S. Tappia and Rajesh Katare
Submitted: 9 December 2025 Revised: 7 April 2026 Accepted: 23 April 2026 Published: 24 June 2026

Abstract

Background: Heart failure (HF) is characterized by mitochondrial dysfunction and immune dysregulation. However, the underlying molecular mechanisms remain unclear. Functional enrichment analyses study aimed to identify key mitochondrial genes involved in HF pathogenesis and to explore their association with immune cell infiltration. **Methods**: Differentially expressed genes related to HF were identified and subjected to functional enrichment analyses. Summary data-based Mendelian randomization (SMR) was used to evaluate the diagnostic potential of candidate genes. Immune cell infiltration analysis was performed to assess associations between gene expression and immune profiles. Single-cell RNA sequencing data (GSE145154) were analyzed to determine cell-specific expression patterns. A transverse aortic constriction (TAC)-induced HF mouse model was established, and cardiac function was assessed by echocardiography. Histopathological analyses were conducted to evaluate myocardial injury, fibrosis, and apoptosis. Immune cell populations were further examined *in vivo*. **Results**: Functional enrichment analysis revealed that HF-related genes were significantly associated with mitochondrial organization and pathways such as mechanistic target of rapamycin (*mTOR*) signaling and cardiomyopathy. SMR analysis identified NADH: ubiquinone oxidoreductase core subunit S2 (*NDUFS2*) and NME/NM23 nucleoside diphosphate kinase 6 (*NME6*) as having diagnostic relevance. Immune infiltration analysis showed correlations between these genes and immune cell populations. Single-cell RNA sequencing revealed that *NME6* was predominantly expressed in T cells and neutrophils, indicating potentially important significance. Clinical data suggested that brain natriuretic peptide (BNP), C-reactive protein (CRP), neutrophils, monocytes, and inflammatory factor levels tended to increase with HF severity. Echocardiography determined that in HF mice, NME6 knockdown lessened the left ventricular end-diastolic diameter (LVEDD) and end-systolic diameter (LVESD) while boosting the left ventricular ejection fraction (LVEF) and fractional shortening (LVFS). Histopathological analysis further demonstrated that *NME6* knockdown alleviated myocardial damage and fibrosis, and inhibited cardiomyocyte apoptosis in HF mice. In-depth studies indicated that *NME6* knockdown mitigated HF by increasing the proportion of $CD4^+$ T cells and decreasing the proportions of $CD8^+$ T cells and $CD44^+CD62L^+$ T cells. **Conclusions**: NME6 may act as a regulator of immune responses and a potential therapeutic target in HF, providing new insights into the molecular mechanisms of HF.

Keywords: heart failure; mitochondrial dysfunction; *NDUFS2*; *NME6*; immune cell infiltration

1. Introduction

Heart failure (HF) is a clinical illness marked by the heart's lower capacity to pump blood efficiently, which leads to venous congestion and insufficient perfusion of peripheral tissues [1]. The core pathophysiological mechanisms of HF include diminished myocardial contractility and/or excessive cardiac workload [2]. Common clinical symptoms include exertional dyspnea, lower limb edema, and persistent fatigue [3], while more severe cases may present with nocturnal paroxysmal dyspnea and pulmonary edema [4].

Clinically, HF is classified into left- and right-sided HF, depending on the affected ventricle [5]. Left-sided HF primarily results from pulmonary circulatory congestion and is commonly manifested as dyspnea and nocturnal wheezing [6]. In contrast, right-sided HF often arises from pulmonary hypertension or progression of left-sided HF, with hallmark features including peripheral edema and hepatomegaly [7]. Beyond these clinical manifestations, HF involves complex pathophysiological processes such as metabolic disturbances, inflammation, and immune cell infiltration [8]. The prognosis for HF is still not ideal despite advancements in pharmacologic and interventional treat-

ments. Therefore, finding new treatment targets requires understanding the molecular and cellular mechanisms underlying the evolution of HF.

There is growing evidence that mitochondrial dysfunction plays a major role in the development and course of HF [9], particularly through its impact on myocardial energy metabolism [10,11]. In HF, reduced activity of mitochondrial respiratory chain enzymes impairs electron transport efficiency, thereby limiting adenosine triphosphate (ATP) production [12]. This energy deficit directly compromises cardiac contractile and relaxation functions [13]. Among the components of the respiratory chain, mitochondrial complex I dysfunction is a major contributor to ATP depletion [14]. NADH: ubiquinone oxidoreductase core subunit S2 (*NDUFS2*), a core subunit of complex I, facilitates the transfer of electrons from nicotinamide adenine dinucleotide (NADH) to ubiquinone and plays a pivotal role in mitochondrial oxidative phosphorylation [15]. Mutations in *NDUFS2* can lead to complex I deficiency and impaired mitochondrial energy metabolism [16]. For instance, *NDUFS2* deficiency in mouse lung epithelial cells impairs alveolar development and leads to postnatal lethality via activation of the mitochondrial integrated stress response (ISR) [17]. Additionally, the development of dilated cardiomyopathy and mitochondrial dysfunction has been connected with NDUFS2 [18].

Another mitochondrial gene of interest is NME/NM23 nucleoside diphosphate kinase 6 (*NME6*), a member of the nucleoside diphosphate kinase (NDP kinase) family. Localized to mitochondria, *NME6* is involved in maintaining intracellular nucleotide balance [19]. Unlike other *NME* family members, *NME6* is predominantly expressed in metabolically active tissues [20], underscoring its significance in sustaining mitochondrial function and energy homeostasis [21]. However, the expression patterns of *NDUFS2* and *NME6* in HF, along with their relationships to clinical phenotypes, remain poorly understood and warrant further investigation.

Through the integration of transcriptome data with Mendelian randomization analysis, our goal was to methodically clarify the role of mitochondria-related genes in the development and progression of HF. Specifically, we utilized both bulk and single-cell RNA sequencing (scRNA-seq) datasets from the Gene Expression Omnibus (GEO) to identify mitochondrial genes that are differentially expressed in HF, assess their functional pathways, and evaluate their potential as diagnostic biomarkers. Moreover, we investigated the cellular localization of key mitochondrial genes in cardiomyocytes and immune cells, and analyzed their correlations with clinical indicators of inflammation and cardiac dysfunction. Our research may aid in the discovery of novel treatment targets and diagnostic indicators, ultimately leading to the creation of more potent HF management techniques.

2. Materials and Methods

2.1 Differentially Expressed Genes (DEGs) Identification and Functional Annotation in the GSE120895 Dataset

The GSE120895 dataset, containing 47 heart tissue samples from HF patients and 8 control samples, was acquired from the GEO database (https://www.ncbi.nlm.nih.gov/geo). Using the GEO2R program, DEGs were discovered following the selection criterion $|\log_2$ fold change$| > 1$ and p-value < 0.05. The Database for Annotation, Visualization and Integrated Discovery (DAVID) database (https://davidbioinformatics.nih.gov/) was implemented for functional enrichment analysis, consisting of Gene Ontology (GO) and Kyoto Encyclopedia of Genes and Genomes (KEGG) pathway analysis.

2.2 Identification of HF-Associated Mitochondrial Genes via Summary-Data-Based Mendelian Randomization (SMR)

The MitoCarta3.0 database (https://www.broadinstitute.org/mitocarta) included 1136 genes relevant to mitochondrial function, which were then evaluated for expression in the GSE120895 dataset. To identify HF-associated mitochondrial genes, genome-wide association study (GWAS) summary statistics were obtained from the MRC-IEU database (977,323 European individuals, HF phenotype; ebi-a-GCST009541, https://gwas.mrcieu.ac.uk/), and expression quantitative trait loci (eQTL) data were retrieved from the eQTLGen Phase 1 database (n = 31,684; https://eqtlgen.org/phase1.html). SMR analysis was performed using SMR software (v1.3.1, Yang Lab, Westlake University, Hangzhou, Zhejiang, China). To eliminate single-nucleotide polymorphisms (SNPs) with potential horizontal pleiotropy, the heterogeneity in dependent instruments (HEIDI) test was applied. Genes with $p\_\text{SMR} < 0.05$ and $p\_\text{HEIDI} > 0.01$ were considered statistically significant.

2.3 Identification and Expression Validation of HF-Related Mitochondrial Genes

To find the overlap between DEGs and mitochondrial genes found by SMR, a Venn diagram was created using the online tool (http://bioinformatics.psb.ugent.be/webtools/Venn/). This allowed for the screening of mitochondrial genes linked to HF. The expression profiles of five intersecting genes (HtrA serine peptidase 2 (*HTRA2*), *NDUFS2*, *NME6*, tRNA methyltransferase 10C, mitochondrial RNase P subunit (*TRMT10C*), tRNA methyltransferase 61B (*TRMT61B*)) were subsequently validated using the Sangerbox online platform (http://vip.sangerbox.com) based on the GSE120895 dataset.

2.4 Diagnostic Value and Pathway Enrichment Analysis of Candidate Mitochondrial Genes

To assess the diagnostic potential of NDUFS2 and NME6 in HF, receiver operating characteristic (ROC) curve analysis was done using the pROC package (v1.18.0) in R

(R Foundation for Statistical Computing, Vienna, Austria). To gauge diagnostic performance, the area under the curve (AUC) was computed. Based on the median gene expression, samples were divided into groups with high and low expression. To investigate functional pathways connected to these candidate genes, Gene Set Enrichment Analysis (GSEA, v3.0) was carried out using the KEGG gene sets (c2.cp.kegg.v7.4.symbols.gmt) from the Molecular Signatures Database (MSigDB; http://www.gsea-msigdb.org/gsea/downloads.jsp) [22].

2.5 Immune Cell Infiltration Analysis and Correlation With Mitochondrial Gene Expression

The CIBERSORTx algorithm and the LM22 signature matrix served to figure out the immune cell composition in HF samples from the GSE120895 dataset. The relative proportions of 22 immune cell types were estimated using a total of 1000 permutations. The relationships between NDUFS2 and NME6 and immune cell infiltration levels were evaluated through Pearson correlation analysis. The ggplot2 package in R was applied to visualize the data (https://cran.r-project.org/package=ggplot2).

2.6 Single-Cell RNA Sequencing (scRNA-seq) Data Processing and Quality Control

Four HF patients' left ventricular tissue scRNA-seq data (GSE145154) were obtained from the GEO dataset. The Seurat R package (v4.0.1, Satija Lab, New York Genome Center, New York, NY, USA) was implemented to process the data. Cells with mitochondrial gene content greater than 20% or those expressing fewer than 200 or more than 10,000 genes were eliminated. Additionally, genes expressed in fewer than three cells were eliminated. For further examination, the top 3000 highly variable genes were chosen. Principal component analysis (PCA) was carried out by batch effects correction using the Harmony algorithm (v0.1.0, Broad Institute of MIT and Harvard, Cambridge, MA, USA), then clustering and dimensionality reduction were performed based on the top 20 principal components. Key quality metrics—including hemoglobin gene percentage (HB_percent), mitochondrial gene percentage (mt_percent), nFeature_RNA, and nCount_RNA—were visualized for each sample.

2.7 Cell Type Annotation and Gene Expression Visualization

Uniform manifold approximation and projection (UMAP) based on the top 20 Harmony-corrected components was used for dimensionality reduction. 15 clusters were produced by cell clustering using Seurat's FindClusters function with a resolution of 0.8. The FindAllMarkers program was applied to identify marker genes, and the CellMarker database was consulted for cell type annotation. Cardiomyocytes, fibroblasts, endothelial cells, B cells, T cells, natural killer (NK) cells, neutrophils, monocytes, macrophages, and myeloid cells were among the cell types that were identified. The expression and distribution of *NDUFS2* and *NME6* across different cell types were visualized using UMAP feature plots and violin plots.

2.8 Clinical Sample Collection and Inflammatory Marker Assessment

Thirty patients diagnosed with HF were recruited from the First Affiliated Hospital of Anhui University of Traditional Chinese Medicine between January and December 2023. Inclusion criteria were: (1) diagnosis of HF according to the 2021 European Society of Cardiology (ESC) guidelines; (2) available echocardiographic data for left ventricular ejection fraction (LVEF); and (3) signed informed consent. Patients were categorized into New York Heart Association (NYHA) functional classes I (n = 1), II (n = 5), III (n = 20), and IV (n = 4). Peripheral venous blood samples were collected at admission. Plasma brain natriuretic peptide (BNP) levels were measured by chemiluminescence immunoassay, while serum C-reactive protein (CRP) was determined using immunoturbidimetry. Neutrophil and monocyte counts were obtained using an automated hematology analyzer (Sysmex XN-9000, Sysmex, Kobe, Japan). This study was approved by the Medical Ethics Committee of the First Affiliated Hospital of Anhui University of Traditional Chinese Medicine (2022AH-93), and all procedures adhered to the Declaration of Helsinki. Written informed consent was obtained from all participants.

To evaluate the inflammatory response in HF patients, blood samples from the aforementioned 30 HF patients and 20 healthy controls were collected, and the supernatants were obtained after centrifugation. Subsequently, enzyme-linked immunosorbent assay (ELISA) kits were used to measure the serum levels of interleukin-6 (IL-6, PI330, Beyotime, Shanghai, China), transforming growth factor-alpha (TNF-α, PT518, Beyotime, Shanghai, China), interleukin-1 beta (IL-1β, PI305, Beyotime, Shanghai, China), and tumor necrosis factor-beta (TGF-β, PT880, Beyotime, Shanghai, China).

2.9 Quantitative Real-Time Polymerase Chain Reaction (qRT-PCR)

Peripheral blood mononuclear cells from HF patients or mouse heart tissues were collected, and total RNA was extracted using Trizol (R0016, Beyotime, Shanghai, China). Subsequently, the RNA was reverse-transcribed into cDNA using the PrimeScript™ RT reagent Kit (RR037Q, Takara, Kusatsu, Shiga, Japan). The qRT-PCR reaction was then performed and analyzed using a 2× SYBR Green kit (11201ES03, Yeasen, Shanghai, China). The $2^{-\Delta\Delta CT}$ technique was implemented to calculate relative expression levels, with glyceraldehyde-3-phosphate dehydrogenase (GAPDH) serving as the internal reference gene. The primer sequences are presented in Table 1.

Table 1. Primer names and sequences.

Gene	Forward (5'-3')	Reverse (5'-3')
NME6	ATGGAGCAGCCTGAGGAGC	CTCATCTCCTGCTCCTGCT
GAPDH	CTCTGCTCCTCCCTGTTCGAC	ACGACCAAATCCGTTGACTC

NME6, NME/NM23 nucleoside diphosphate kinase 6; *GAPDH*, Glyceraldehyde-3-phosphate dehydrogenase.

2.10 Western Blot

Peripheral blood mononuclear cells were collected from HF patients or mouse heart tissues. radioimmunoprecipitation assay (RIPA) lysis buffer (P0013B, Beyotime, Shanghai, China) was implemented to extract total protein, and a bicinchoninic acid (BCA) kit (P0009, Beyotime, Shanghai, China) was used to evaluate the protein concentration. After being separated via sodium dodecyl sulfate-polyacrylamide gel electrophoresis (SDS-PAGE, AP2002, Applygen, Beijing, China), the proteins were put onto a polyvinylidene difluoride (PVDF, WJ002, Epizyme, Shanghai, China) membrane. The membrane was blocked for one hour in blocking buffer (P0216, Beyotime, Shanghai, China). It was subsequently transferred to a primary antibody dilution solution and incubated overnight (4 ℃). The membrane was then placed in a solution containing horseradish peroxidase (HRP)-conjugated secondary antibody (SA00001-1, Wuhan, Hubei, Proteintech, China) and incubated for an additional 1 h. Subsequently, the PVDF membrane was developed utilizing an enhanced chemiluminescence (ECL) kit (P0018S, Beyotime, Shanghai, China). The primary antibodies used were anti-NME6 (1:1000, 10250-1-AP, Proteintech, Wuhan, Hubei, China) and anti-GAPDH (1:1000, 60004-1-Ig, Proteintech, Wuhan, Hubei, China).

2.11 Flow Cytometry

Single-cell suspensions from the heart tissues of HF mice. Appropriate amounts of working antibody solutions containing fluorescently-labeled FITC-CD3 (FITC-65504, Proteintech, Wuhan, Hubei, China), FITC-CD44 (FITC-98333-3, Proteintech, Wuhan, Hubei, China), PE-CD4 (PE-65104, Proteintech, Wuhan, Hubei, China), PE-CD8 (PE-65069, Proteintech, Wuhan, Hubei, China), PE-NME6 (10250-1-AP, Proteintech, Wuhan, Hubei, China), PE-CD62L (PE-65219, Proteintech, Wuhan, Hubei, China), and PD-1 (66220-1-Ig, Proteintech, Wuhan, Hubei, China) antibodies were added. The samples were then incubated at 4 °C in the dark for 30 minutes. Subsequently, the cells were resuspended in phosphate-buffered saline (PBS) and analyzed using a flow cytometer (CytoFLEX, Beckman, Brea, CA, USA). The gating strategy for flow cytometry was as follows: first, all debris and dead cells were excluded based on forward scatter (FSC-A) and side scatter (SSC-A). Then, $CD3^+$ T cells were gated from the live cell population. Within the $CD3^+$ T cell gate, $CD4^+$ and $CD8^+$ T cell subsets were further identified. Finally, the expression of NME6, CD62L, and PD-1 was analyzed in each T cell subset. In this study, primary peripheral blood mononuclear cells (PBMCs) were isolated from HF patients, and single-cell suspensions were prepared from mouse heart tissues. These primary cells were used immediately after isolation without *in vitro* expansion.

2.12 Construction and Grouping of HF Mice

Twelve male C57BL/6 mice (6–8 weeks old, 18–22 g), six male C57BL/6 mice with *NME6* knockdown (sh-NME6), and six male littermate control mice (sh-NC) were purchased from Sipeifu (China) and kept in a specific-pathogen-free (SPF) environment. sh-NME6 (pscAAV[shRNA]-EGFP-U6>mNme6[shRNA#1]) was constructed by VectorBuilder (Guangzhou, Guangdong, China) to achieve specific knockdown of NME6. The AAV9 vector (1×10^{11} viral genome particles per mouse) was administered via tail vein injection. Two weeks after viral transduction, the mice underwent model induction. The mice were given unlimited access to food and water, and a 12-hour light/dark cycle was maintained. All mice were randomly allocated to experimental groups using a random number table method. All animal experimental procedures adhered to the ARRIVE 2.0 guidelines and were approved by the Ethics Committee of the First Affiliated Hospital of Anhui University of Traditional Chinese Medicine (AZYFY-2024-1005).

After 7 days of acclimatization, mice were anesthetized and fixed in a supine position. Anesthesia was induced with isoflurane (3%; 26675-46-7, Labgle, Nanjing, China) and maintained with 1.5% isoflurane in 100% oxygen (0.8–1.0 L/min) delivered via a nose cone. Absence of the pedal withdrawal reflex confirmed adequate anesthesia. During the entire surgical procedure, anesthetic depth was continuously monitored by assessing respiratory rate, pedal withdrawal reflex, and corneal reflex, and isoflurane concentration was adjusted as needed to maintain a stable surgical plane of anesthesia. Body temperature was maintained at 37 °C using a thermostatically controlled heating pad, and ophthalmic ointment was applied to prevent corneal drying. Subsequently, the skin on the neck and chest of the mice was incised, and an incision was made at the second intercostal space along the left upper sternal margin. The thymus was separated to expose the aortic arch and its branches, and sutures were passed through and tied around the aortic arch. Next, a 26-G needle was placed adjacent to the aorta, and the suture was tightened. The needle was then

removed, creating a stenotic lumen in the aorta to establish the HF model. Finally, the wound was sutured, and the mice returned to their cages. Perioperative analgesia was provided with buprenorphine (0.05 mg/kg, subcutaneous, MM0120.00-0250, LGC, Teddington, London, UK) administered 30 min prior to surgery and every 12 h for 48 h postoperatively to minimize pain and distress. Mice in the Sham group (n = 6) underwent the same procedures but without ligation. At the study endpoint (4 weeks post-surgery) or when humane endpoints were reached, mice were euthanized by an overdose of sodium pentobarbital (200 mg/kg, 50 mg/mL, intraperitoneal, MM1368.00, LGC, Teddington, London, UK). To minimize bias, all animal handling, treatment administration, and outcome assessments were performed in a blinded manner throughout the experimental period. Loss of consciousness was verified by the absence of corneal and pedal reflexes. Death was confirmed by cessation of respiration and the absence of cardiac activity, followed by cervical dislocation as a secondary method.

2.13 Experimental Echocardiography

An experienced veterinary cardiologist conducted blinded echocardiographic exams four weeks after surgery. Specifically, after anesthetizing the mice and applying a layer of ultrasound transmission gel, transthoracic echocardiography (M-mode) was conducted using an ultrasound machine (iE33, Philips, Best, Noord-Brabant, Netherlands) equipped with a 15 MHz linear array transducer. For echocardiography, mice were maintained under light isoflurane anesthesia (1.0–1.5% in oxygen) delivered via a nose cone. Body temperature was maintained at 37 °C on a heated platform during imaging. M-mode tracings of the left ventricle were acquired at the level close to the papillary muscles using the two-dimensional parasternal short-axis imaging plane as a guide. The M-mode recordings served to determine the LVEF and left ventricular fractional shortening (LVFS). Additionally, measurements were made of the left ventricle's end-diastolic diameter (LVEDD) and end-systolic diameter (LVESD).

2.14 Hematoxylin and Eosin (H&E) Staining

After the feeding period, the mice were dissected to obtain fresh heart tissues, which were then processed to obtain paraffin sections. Subsequently, the sections were immersed in hematoxylin staining solution (ST2067, Beyotime, Shanghai, China) for 5 minutes and differentiated with 1% hydrochloric acid alcohol (C0163M, Beyotime, Shanghai, China) for 30 seconds. Next, the sections were immersed in eosin staining solution (C0109, Beyotime, Shanghai, China) for 5 minutes and then washed to remove any residual dye. The sections were then dehydrated, cleaned, and mounted before being examined under a microscope (Leica, Wetzlar, Hesse, Germany) to look for pathological alterations in the hearts of the mice in each group.

2.15 Masson Staining

The mouse heart tissues were stained using a Masson's Trichrome Staining Kit (C0189S, Beyotime, Shanghai, China). Specifically, the tissue sections were placed in hematoxylin staining solution for 5 minutes and differentiated with hydrochloric acid-alcohol differentiation solution for 30 seconds. Subsequently, the sections were transferred to a Ponceau-acid fuchsin solution for 10 minutes and then a light green staining solution for 1 minute. Finally, after being dehydrated, cleared, and mounted, the sections were observed under a microscope to measure the area of blue-stained regions.

2.16 Terminal Deoxynucleotidyl Transferase dUTP Nick End Labeling (TUNEL) Staining

The TdT enzyme reaction combination was made in accordance with the directions for the TUNEL Assay Kit (C1091, Beyotime, Shanghai, China) in order to assess the effect of NME6 on cardiomyocyte apoptosis in mice with HF. The mixture was then applied to the sections and left to incubate for 60 minutes (37 °C) in the dark. Following incubation, PBS was utilized to remove any remaining dye, and fluorescence pictures were taken under a fluorescence microscope (Leica, Wetzlar, Hesse, Germany).

2.17 Measurement of Mouse Cardiac Function

To evaluate cardiac function in mice, the serum levels of cardiac troponin T (cTnT) (XZK-9711, Xuanzekang, Shanghai, China), BNP (EL-M0166, Elabscience, China), and atrial natriuretic peptide (ANP) (EL-M0204, Elabscience, Wuhan, Hubei, China) were measured using the ELISA method. Specifically, mouse blood was collected, centrifuged, and the supernatant was obtained. Subsequently, reaction reagents were added in sequence as per the manufacturer's protocols, and the absorbance at 450 nm was measured using a microplate reader (BioTek, Winooski, Vermont, USA).

2.18 Measurement of Inflammatory Cytokine Levels

To evaluate the inflammatory response in mice with HF, the serum levels of IL-6 (PI326, Beyotime, China), TNF-α (PT512, Beyotime, Shanghai, China), and interferon-gamma (IFN-γ, PI508, Beyotime, Shanghai, China) were measured using the ELISA method. Specifically, mouse serum was prepared, and the reaction reagents were added in sequence following the manufacturer's protocols. A microplate reader was subsequently utilized to assess the absorbance (450 nm).

2.19 Immunofluorescence

Mouse heart tissue sections were immersed in citrate buffer (pH = 6.0, C9999, Beyotime, Shanghai, China) and subjected to antigen retrieval by microwave heating for 20 minutes. After retrieval, the sections were transferred to a 3% H_2O_2 solution (P0100A, Beyotime, Shanghai, China) to

block endogenous peroxidase activity. Subsequently, they were placed in 10% goat serum (C0265, Beyotime, Shanghai, China) for 1 h. After blocking, the sections were incubated with CD3 antibody (60181-1-Ig, Proteintech, Wuhan, Hubei, China) and NME6 antibody (ym-c7617R, Yuanmu, Shanghai, China) overnight (4 °C). The next day, the sections were immersed in fluorescently labeled secondary antibodies and further incubated for 1 h. They were then removed and immersed in 4′,6-diamidino-2-phenylindole (DAPI, 40728ES03, Yeasen, Shanghai, China) staining solution for 15 minutes. Finally, the sections were observed under a fluorescence microscope.

2.20 Statistical Analysis

R (v4.1.2, R Foundation for Statistical Computing, Vienna, Austria) and GraphPad Prism (v9.0, GraphPad Software, LLC, San Diego, CA, USA) served for all statistical analyses. The mean ± standard error of the mean (SEM) is implemented to display the data. One-way analysis of variance (ANOVA) and Tukey's post hoc test served to evaluate differences between several groups. Statistical accuracy was defined as a p-value of less than 0.05. Post-hoc power analysis was conducted using G*Power (one-way ANOVA, fixed-effects) for cardiac functional, molecular, biochemical, and histopathological endpoints, including LVEF, LVFS, LVESD, LVEDD, myocardial injury markers (cTnT, BNP, ANP) and inflammatory cytokines (IL-6, TNF-α, IFN-γ). For the primary endpoint (LVEF), with $\alpha = 0.05$ and $n = 6$ per group, the observed effect size $f = 2.10$ corresponded to a statistical power of 100%, indicating that the sample size was sufficient to reliably detect significant differences among the four groups. Secondary endpoints generally exhibited smaller effect sizes and slightly lower power; however, the direction and magnitude of effects were consistent across related indices, supporting the biological robustness of the findings.

3. Results

3.1 Functional Enrichment Analysis Reveals Involvement of Mitochondria-Related DEGs in Mitochondrial Signaling Pathways

From the GSE120895 dataset, 7109 upregulated and 394 downregulated genes were found. The top 50 DEGs are presented in Fig. 1A. Functional enrichment analysis, conducted using the DAVID database, indicated significant enrichment of terms related to mitochondrial biology. These included "regulation of mitochondrion organization", "protein targeting to mitochondrion", "mitochondrion organization", "autophagy of mitochondrion", and "mitochondrion transport along microtubule" (Biological Process, BP); "cytosol" and "mitochondrion" (Cellular Component, CC); as well as "ubiquitin protein ligase binding" and "RNA binding" (Molecular Function, MF) (Fig. 1B–D). Analysis of the KEGG pathway also showed a notable enrichment in "cellular senescence", "mTOR signaling pathway", and cardiac-related pathways, such as "hypertrophic cardiomyopathy" and "dilated cardiomyopathy" (Fig. 1E). The results suggest the identified DEGs may contribute to HF pathogenesis, particularly via mitochondrial dysfunction and myocardial remodeling.

3.2 Identification of HF-Associated Mitochondrial Genes via SMR and Transcriptomic Analysis

To further explore the involvement of mitochondrial genes in HF, 1136 genes were retrieved from the MitoCarta3.0 database, of which 1096 were found in the GSE120895 dataset. Their expression profiles in HF and control samples were visualized using a heatmap (**Supplementary Fig. 1**). To identify potentially causal mitochondrial genes, SMR analysis combined with the HEIDI test was performed using GWAS data from 977,323 European individuals and eQTL data from the eQTLGen phase 1 dataset. Seven mitochondrial genes were significantly associated with the risk of HF (Table 2). Elevated expression levels of thioesterase superfamily member 5 (*THEM5*) (OR = 1.278), *NDUFS2* (OR = 1.086), translocase of outer mitochondrial membrane 40 like (*TOMM40L*) (OR = 1.105), and *NME6* (OR = 1.073) were favorably correlated with the risk of HF, while higher expression levels of *TRMT61B* (OR = 0.925), *HTRA2* (OR = 0.832), and *TRMT10C* (OR = 0.699) were inversely associated, suggesting a protective role.

3.3 Diagnostic Potential and Enrichment Analysis of HF-Related Mitochondrial Genes

Cross-analysis between the 7 SMR-identified genes and GSE120895-derived DEGs yielded 5 candidate genes (*NDUFS2*, *TRMT61B*, *HTRA2*, *NME6*, *TRMT10C*) that were significantly associated with HF (Fig. 1F–K). Elevated levels of these genes in HF samples were confirmed by expression analysis. ROC analysis showed that *NDUFS2* (AUC = 0.816) and *NME6* (AUC = 0.875) exhibited strong diagnostic value. GSEA indicated that *NDUFS2* was substantially engaged in metabolic and HF-related pathways such as "pyruvate metabolism", "hypertrophic cardiomyopathy", "insulin signaling pathway", "adipocytokine signaling pathway", and "peroxisome proliferator-activated receptor (PPAR) signaling pathway" (Fig. 1L–N). Likewise, *NME6* was enriched in mitochondrial and cardiac-related pathways, including "oxidative phosphorylation", "valine, leucine and isoleucine biosynthesis", "riboflavin metabolism", "arginine and proline metabolism", and "cardiac muscle contraction" (Fig. 1N).

3.4 NDUFS2 and NME6 Show Distinct Correlations With Immune Cell Infiltration in HF

Analysis of immune cell infiltration based on GSE120895 transcriptomic data identified differential proportions of 22 immune cell subtypes between HF and control samples (Fig. 2A). Pearson correlation analysis

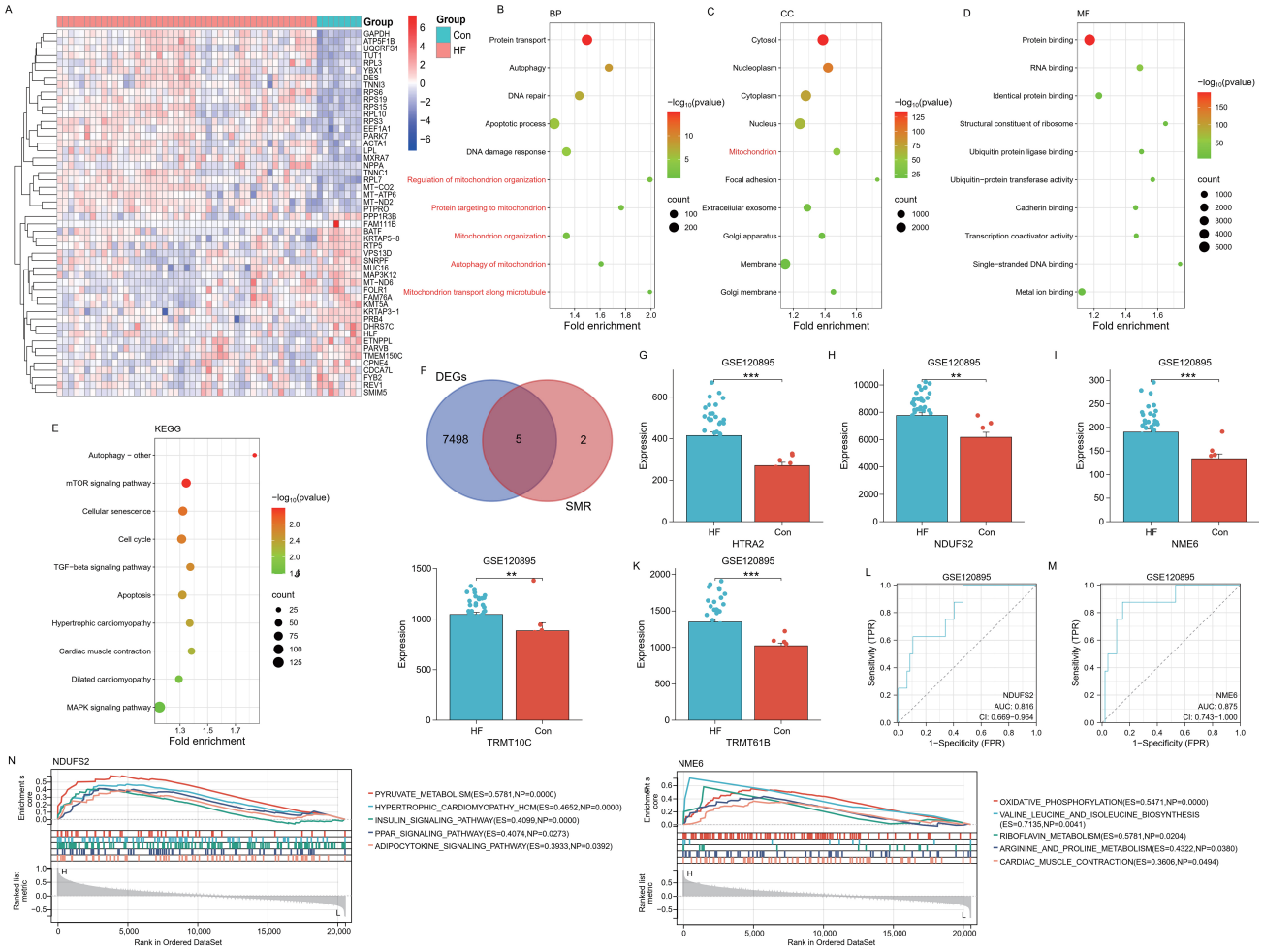

Fig. 1. Diagnostic performance and pathway enrichment analysis of the mitochondrial genes NADH: ubiquinone oxidoreductase core subunit S2 (*NDUFS2*) and NME/NM23 nucleoside diphosphate kinase 6 (*NME6*) in heart failure (HF). (A) Heat map of differential expression of the top 50 genes in the HF group and the control group (Con) in the GSE120895 dataset. Red indicates upregulation; blue indicates downregulation. (B–E) Biological process (BP), cellular component (CC), molecular function (MF), and Kyoto Encyclopedia of Genes and Genomes (KEGG) pathway enrichment analysis of differentially expressed genes (DEGs) in the GSE120895 dataset. The size of the point represents the number of genes, while the color scale indicates the statistical significance ($-\log_{10}$ [*p*-value]). The terms related to mitochondria are highlighted in red. (F) Venn diagram, intersection analysis between DEGs in the GSE120895 dataset and mitochondrial candidate genes obtained based on summary-based Mendelian randomization (SMR) analysis. (G–K) Bar graphs showing the expression levels of 5 intersection genes in HF and Con group samples based on the GSE120895 dataset, including HtrA serine peptidase 2 (*HTRA2*) (G), *NDUFS2* (H), *NME6* (I), tRNA methyltransferase 10C, mitochondrial RNase P subunit (*TRMT10C*) (J), and tRNA methyltransferase 61B (*TRMT61B*) (K). (L,M) Receiver operating characteristic (ROC) curves for *NDUFS2* (L) and *NME6* (M) based on the GSE120895 dataset. The area under the curve (AUC) was 0.816 (95% CI: 0.669–0.964) for *NDUFS2* and 0.875 (95% CI: 0.743–1.000) for *NME6*, indicating the two genes have strong discriminatory power in distinguishing HF from control samples. CI, Confidence interval. (N) Gene set enrichment analysis (GSEA) of the expression levels of *NDUFS2* and *NME6*. The enrichment plots show the significantly enriched KEGG pathways ranked by enrichment score (ES). $^{**}p < 0.01$, $^{***}p < 0.001$.

between gene expression and immune cell proportions revealed that *NDUFS2* expression was positively correlated with memory B cells (r = 0.35), naïve $CD4^+$ T cells (r = 0.29) and resting mast cells (r = 0.20), and negatively correlated with naïve B cells (r = –0.48), resting memory $CD4^+$ T cells (r = –0.33), and activated memory $CD4^+$ T cells (r = –0.26). In contrast, *NME6* expression showed positive correlations with $CD8^+$ T cells (r = 0.20), naïve $CD4^+$ T cells (r = 0.38), and eosinophils (r = 0.19), while negatively correlating with naïve B cells (r = –0.23), resting memory $CD4^+$ T cells (r = –0.31), M1 macrophages (r = –0.20), and resting dendritic cells (r = –0.27) (Fig. 2B). These results suggest that mitochondrial gene dysregulation may influence the immune microenvironment in HF.

Table 2. Mitochondria-related gene expression and HF GWAS data.

Gene	TopSNP	β coefficient	OR	CI_lower	CI_upper	*p*_SMR	*p*_HEIDI
THEM5	rs11204901	0.245	1.278	1.066	1.533	0.008	0.014
NDUFS2	rs4379692	0.082	1.086	1.009	1.168	0.028	0.200
TOMM40L	rs5082	0.100	1.105	1.045	1.168	0.000	0.077
TRMT61B	rs55785599	–0.077	0.925	0.871	0.983	0.012	0.943
HTRA2	rs72470544	–0.183	0.832	0.701	0.988	0.036	0.718
NME6	rs11718350	0.071	1.073	1.003	1.148	0.040	0.376
TRMT10C	rs9825208	–0.358	0.699	0.519	0.942	0.019	0.160

GWAS, genome-wide association study; SNP, single-nucleotide polymorphism; SMR, summary data-based Mendelian randomization; OR, odds ratio; CI, confidence interval; HEIDI, heterogeneity in dependent instruments; *THEM5*, thioesterase superfamily member 5; *TOMM40L*, translocase of outer mitochondrial membrane 40 like.

3.5 Quality Control and Dimensionality Reduction of Single-Cell RNA Sequencing in Failing Left Ventricular Tissue

To investigate cell type-specific gene expression changes in HF, we analyzed scRNA-seq data from four left ventricular tissue samples (GSM4307520, GSM4307525, GSM4307535, GSM4307540) from the GSE145154 dataset. After applying stringent quality control criteria, the key quality metrics (nFeature_RNA, nCount_RNA, mitochondrial gene percentage, and hemoglobin gene percentage) were visualized using violin plots, indicating comparable data quality across samples (Fig. 2C). Batch effects between samples were found with the help of PCA (Fig. 2D). These were effectively mitigated using the Harmony package, as shown by reduced component variance (Fig. 2E).

3.6 Single-Cell Clustering and Expression of NDUFS2 and NME6 in Specific Cardiac Cell Types

Unsupervised clustering using the UMAP algorithm identified 15 distinct cell populations in the left ventricular tissue (Fig. 2F). Cell type annotation based on marker gene analysis and the CellMarker database revealed major cardiac and immune cell types, including B cells, cardiomyocytes, endothelial cells, fibroblasts, macrophages, monocytes, myeloid cells, neutrophils, NK cells, and T cells (Fig. 2G). UMAP feature plots indicated that *NDUFS2* was broadly expressed across multiple cell types (Fig. 2H), whereas *NME6* expression was more restricted (Fig. 2I). *NDUFS2* was strongly expressed in macrophages, monocytes, neutrophils, and T cells, but had low expression in endothelial cells and cardiomyocytes (**Supplementary Fig. 2A**). In contrast, *NME6* was predominantly expressed in T cells, with some expression in NK cells and neutrophils, and lower expression in other cell types (**Supplementary Fig. 2B**). These results indicate that *NDUFS2* and *NME6* are differentially expressed among cardiac and immune cell populations, suggesting roles in HF-related cellular heterogeneity.

3.7 Progressive Inflammatory Dysregulation and NME6-Associated T Cell Shifts Across NYHA Classifications in HF

To further assess the relationship between cardiac function and systemic inflammation, we analyzed peripheral blood samples from 30 patients clinically diagnosed with HF, stratified by NYHA grades I–IV. Due to the limited and uneven distribution of patients across NYHA classes, the following analyses are presented in a descriptive and exploratory manner. BNP levels appeared to increase from grade I to IV, suggesting a trend toward worsening cardiac load and ventricular strain (**Supplementary Fig. 3A**). Concurrently, CRP levels showed a similar increasing pattern (**Supplementary Fig. 3B**). Moreover, patients with higher HF grades tended to exhibit higher circulating neutrophil (**Supplementary Fig. 3C**) and monocyte counts (**Supplementary Fig. 3D**). These observations suggest a potential association between HF severity and systemic inflammatory status, although no formal statistical inference was performed due to sample limitations. Consequently, we measured the serum levels of inflammatory cytokines in patients with HF classified as NYHA grades I–IV. The results showed that inflammatory cytokines (IL-6, TNF-α, IL-1β, TGF-β) were elevated across HF patients and exhibited an apparent increasing tendency with higher NYHA grades (Fig. 3A–D).

Previous studies have demonstrated that *NME6* may be associated with the onset and progression of HF, and it is mainly expressed in T cells and neutrophils. Clarifying the role of *NME6* in the treatment of HF through immune regulation holds significant importance. Consequently, we measured the expression of *NME6* in peripheral blood mononuclear cells of patients. The results indicated that NME6 expression varied across patients and showed an apparent upward tendency in individuals with more advanced NYHA classifications (Fig. 3E–G).

To clarify the association between NME6 and T cells, we utilized flow cytometry to measure the proportions of T cell subsets. The results showed that patients with higher NYHA grades tended to present with lower proportions

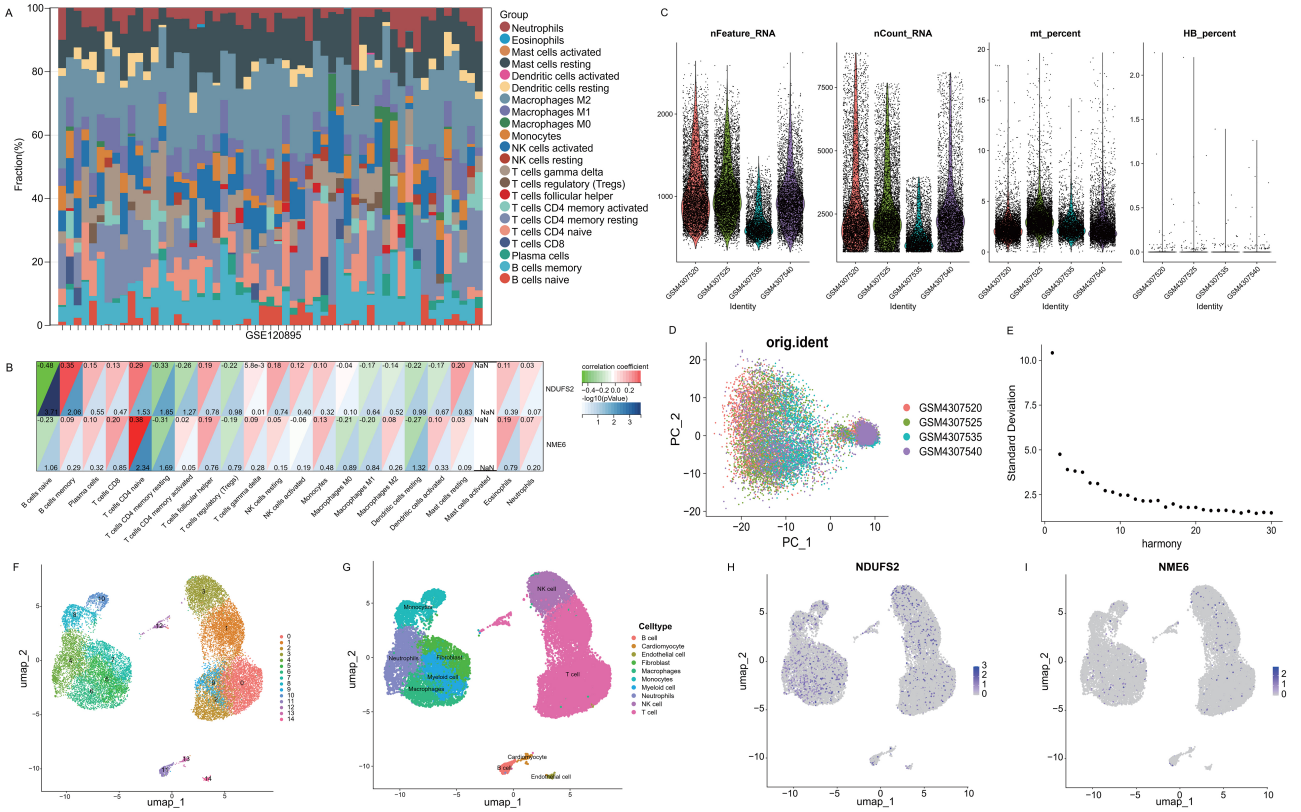

Fig. 2. Cell clustering, cell type annotation, and mitochondrial gene expression in HF single-cell RNA sequencing data. (A) Bar chart showing the relative proportions of 22 immune cell subtypes estimated by the CIBERSORTx algorithm using the LM22 signature in the GSE120895 dataset. (B) Heat map showing the Pearson correlation between *NDUFS2* and *NME6* expression levels and the infiltration levels of 22 immune cell types. The color scale indicates the strength and direction of the correlation, and significance is expressed as –log10 (*p*-value). (C) Violin plots show the distribution of quality control indicators in four HF samples in the GSE145154 dataset, including the number of genes detected (nFeature_RNA), transcript counts (nCount_RNA), mitochondrial gene percentage (mt_percent), and hemoglobin gene percentage (HB_percent). (D) Principal component analysis (PCA) plot showing the distribution of cells along the first two principal components (PC_1 and PC_2) for four HF samples (GSM4307520, GSM4307525, GSM4307535, and GSM4307540) before batch correction. Each point represents a cell. (E) Standard deviation plot showing the batch correction performance based on Harmony. The y-axis represents the standard deviation of cells along the Harmony component, and the x-axis represents the continuous Harmony dimension. (F) Uniform manifold approximation and projection (UMAP) plots showing clustering of single-cell transcriptomes of left ventricular tissue reveal 15 distinct cell subsets. (G) Cell type annotation of clusters based on the top 10 differentially expressed genes (DEGs) and referenced to the CellMarker database, including B cells, cardiomyocytes, endothelial cells, fibroblasts, macrophages, monocytes, myeloid cells, neutrophils, natural killer (NK) cells, and T cells. (H,I) UMAP feature plots displaying the expression levels of *NDUFS2* (H) and *NME6* (I) across all single cells.

of CD4$^+$ T cells and higher proportions of CD8$^+$ T cells. Furthermore, we measured the expression of NME6 in total T cells. The results indicated that NME6 expression displayed a gradual increasing pattern across NYHA classifications (Fig. 3H–M). Overall, these findings provide preliminary evidence suggesting a potential link between NME6 expression, T cell distribution, and inflammatory status in HF; however, these observations require validation in larger and better-balanced clinical cohorts.

3.8 NME6 Knockdown Reverses Cardiac Remodeling and Restores Function in a Murine HF Model

To verify that *NME6* is a potential therapeutic target for HF, we created a mouse HF model by transverse aortic constriction. Compared with the Sham group, the levels of LVEF and LVFS in the HF group were significantly decreased (Fig. 4A–C), while LVEDD and LVESD were substantially raised (Fig. 4D,E), demonstrating the HF mouse model's effective establishment. Knockdown of *NME6* reversed this trend, significantly reducing LVEDD and LVESD, increasing LVEF and LVFS, and alleviating the HF status. We then assessed the NME6 in mouse car-

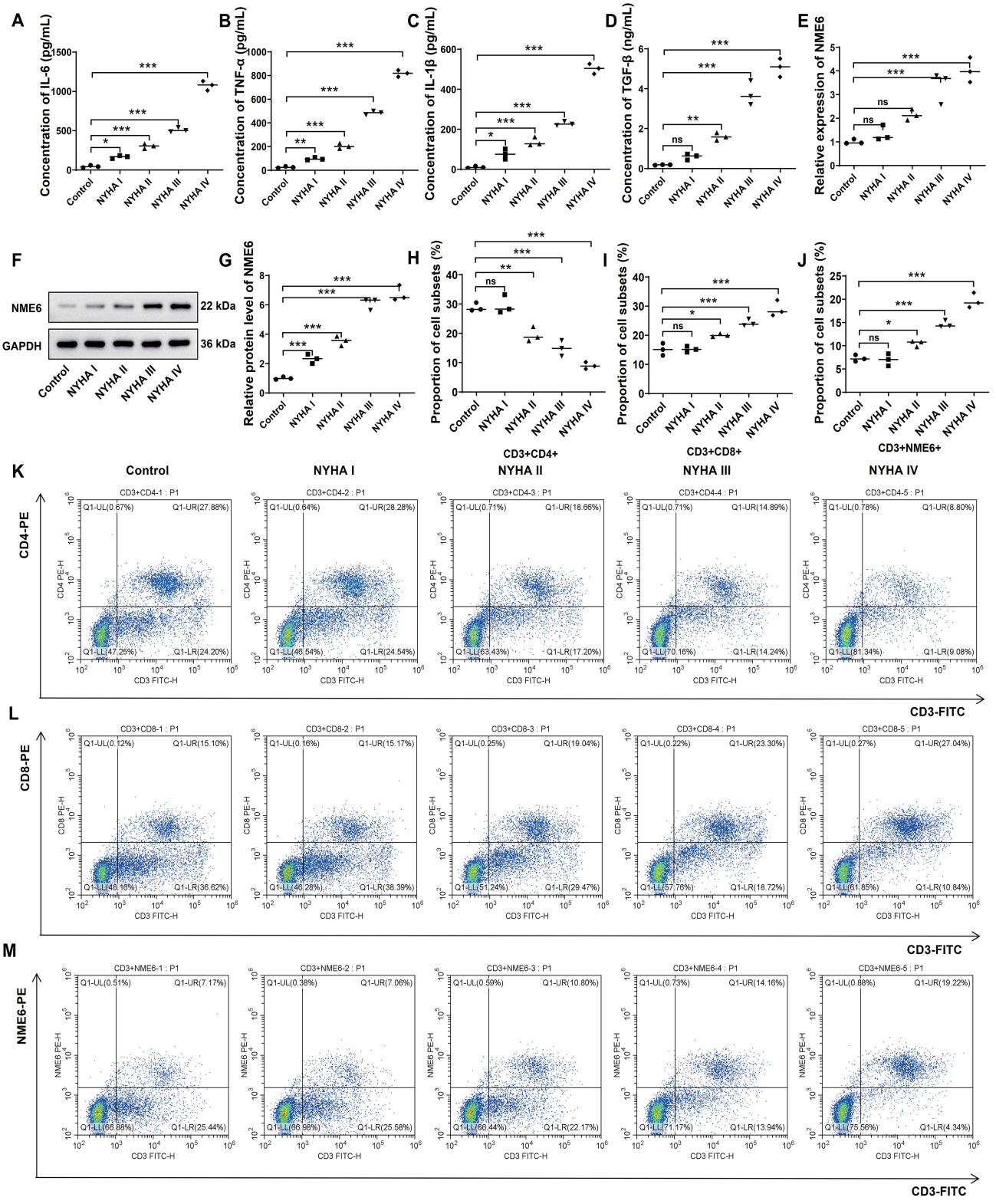

Fig. 3. *NME6* is positively correlated with New York Heart Association (NYHA) classification and can regulate the distribution of T cell subsets. (A–D) Levels of inflammatory cytokines in the serum of HF patients (A) interleukin-6 (IL-6), (B) tumor necrosis factor-alpha (TNF-α), (C) interleukin-1 beta (IL-1β), and (D) transforming growth factor-beta (TGF-β). (E) *NME6* mRNA expression levels in peripheral blood mononuclear cells (PBMCs) of HF patients. (F,G) *NME6* protein expression levels in PBMCs of HF patients. (H–M) Flow cytometry was used to measure the proportions of $CD3^{+}CD4^{+}$ cells, $CD3^{+}CD8^{+}$ cells, and $CD3^{+}NME6^{+}$ cells. ns: not significant, $^{*}p < 0.05$, $^{**}p < 0.01$, $^{***}p < 0.001$.

diac tissues. The successful installation of NME6 knockdown mice was demonstrated by the greatly boosted level of NME6 in the hearts of HF mice compared to the Sham group, whereas it was substantially lower in the HF+sh-NME6 group (Fig. 4F–H).

Next, we calculated the mice's heart weight to body weight ratio (HW/BW). This ratio was considerably lower in the NME6 knockdown group and considerably greater in the HF group as compared to the Sham group (Fig. 4I).

We further evaluated the therapeutic effect of *NME6* knockdown on HF mice by measuring the levels of cTnT, BNP, and ANP. These levels were noticeably higher in HF mice compared with the Sham group. Moreover, *NME6* knockdown diminished the levels of these indicators (Fig. 4J–L), suggesting that it can alleviate myocardial injury in mice. We also performed TUNEL staining on the mouse heart tissues. The Sham group exhibited low green fluorescence intensity, indicating a small number of apoptotic cells. When compared to the Sham group, the HF group had a great deal more apoptotic cells, while NME6 knockdown diminished apoptosis (Fig. 4N,O).

Next, we conducted H&E staining on the mouse hearts. In the Sham group, the myocardial cells were arranged neatly with no obvious pathological symptoms. In the HF group, myocardial cells were arranged in a disordered pattern, with some showing morphological changes and infiltration of inflammatory cells. In contrast, the morphology of myocardial cells was partially restored in the sh-NME6 group, and the number of necrotic myocardial cells was significantly lower (Fig. 4P). Masson staining further demonstrated large areas of blue regions in tissue sections from the HF group and the HF+sh-NC group, indicating severe fibrosis in the hearts of HF mice. The area of the blue region was significantly reduced in the *NME6* knockdown group (Fig. 4M,Q).

3.9 NME6 Knockdown Alleviates HF and Inflammatory Responses by Regulating the Distribution of T Cell Subsets

Prior research has shown that by controlling the immunological milieu, NME6 knockdown can affect T cell subset distribution and reduce inflammatory reactions. Consequently, we measured the impact of *NME6* knockdown on the inflammatory response in HF mice. Serum levels of IFN-γ, TNF-α, and IL-6 were found to be considerably greater in HF animals than in the Sham group. Additionally, NME6 knockdown lessens the inflammatory response in HF animals by lowering the levels of these inflammatory cytokines (Fig. 5A–C).

Based on the preceding research, we hypothesized that alleviation of inflammatory responses in HF by *NME6* knockdown may be associated with the regulation of T cells. We found that the HF group had considerably more $CD3^+NME6^+$ cells than the Sham group using CD3 and NME6 immunofluorescence labeling, indicating that NME6 up-regulates T cells in the cardiac tissues of HF animals (Fig. 5D,E). In contrast, *NME6* knockdown considerably diminished $CD3^+NME6^+$ signals (puncta), confirming the positive correlation between *NME6* and T cell–related immunofluorescence signals (Fig. 5D,E). Compared with the Sham group, the HF model group exhibited a significant decrease in the proportion of $CD3^+CD4^+$ T cells, accompanied by increases in the proportions of $CD3^+CD8^+$ T cells and $CD44^+CD62L^+$ T cells (Fig. 5F–K). NME6 knockdown reversed these HF-induced changes (Fig. 5F–K). Compared with the Sham group, the proportion of PD-1 was increased in the HF group, whereas NME6 knockdown markedly reversed the HF-induced increase in the proportion of PD-1 (Fig. 5L).

4. Discussion

HF is increasingly recognized as a bioenergetic disorder [23], with mitochondrial dysfunction playing a central role in its pathophysiology through altered mitochondrial dynamics, a greater amount of reactive oxygen species (ROS), and disrupted energy production [1,2]. In order to discover mitochondrial genes implicated in HF and explore their possible functions in immunological and metabolic control, we performed a thorough analysis in this work that integrated transcriptome data, SMR analysis, immune cell infiltration, and scRNA-seq.

Transcriptomic analysis of the GSE120895 dataset revealed that HF-associated DEGs were significantly enriched in mitochondrial-related biological processes such as mitochondrial organization, mitophagy, and mitochondrial structure maintenance [24]. KEGG analysis further implicated these genes in key pathways, including the mTOR signaling pathway, cellular senescence, and cardiomyopathy-related pathways, reinforcing the notion that mitochondrial remodeling and quality control are integral to HF development.

Through SMR analysis, we identified five mitochondrial genes significantly associated with HF, with *NDUFS2* and *NME6* emerging as the most relevant due to their up-regulation in HF and their robust diagnostic performance. Both genes showed enrichment in important metabolic pathways such as oxidative phosphorylation and pyruvate metabolism, suggesting involvement in sustaining myocardial energy homeostasis [25]. Existing evidence supports a role for *NDUFS2* in maintaining mitochondrial function and redox balance [26]. Dysfunctional *NDUFS2* impairs complex I activity and promotes ROS accumulation, contributing to impaired contractility and myocardial damage, as shown in dilated cardiomyopathy and other conditions [27]. *NME6* is involved in pyrimidine nucleotide salvage and supports mitochondrial transcription and DNA stability [19,20,21]. NME6 dysregulation has been connected to immunological modulation and a poor outcome in cancer [28]. While these findings hint at their mechanistic importance, the precise functional roles of NDUFS2 and NME6 in HF remain to be fully elucidated. We also investigated

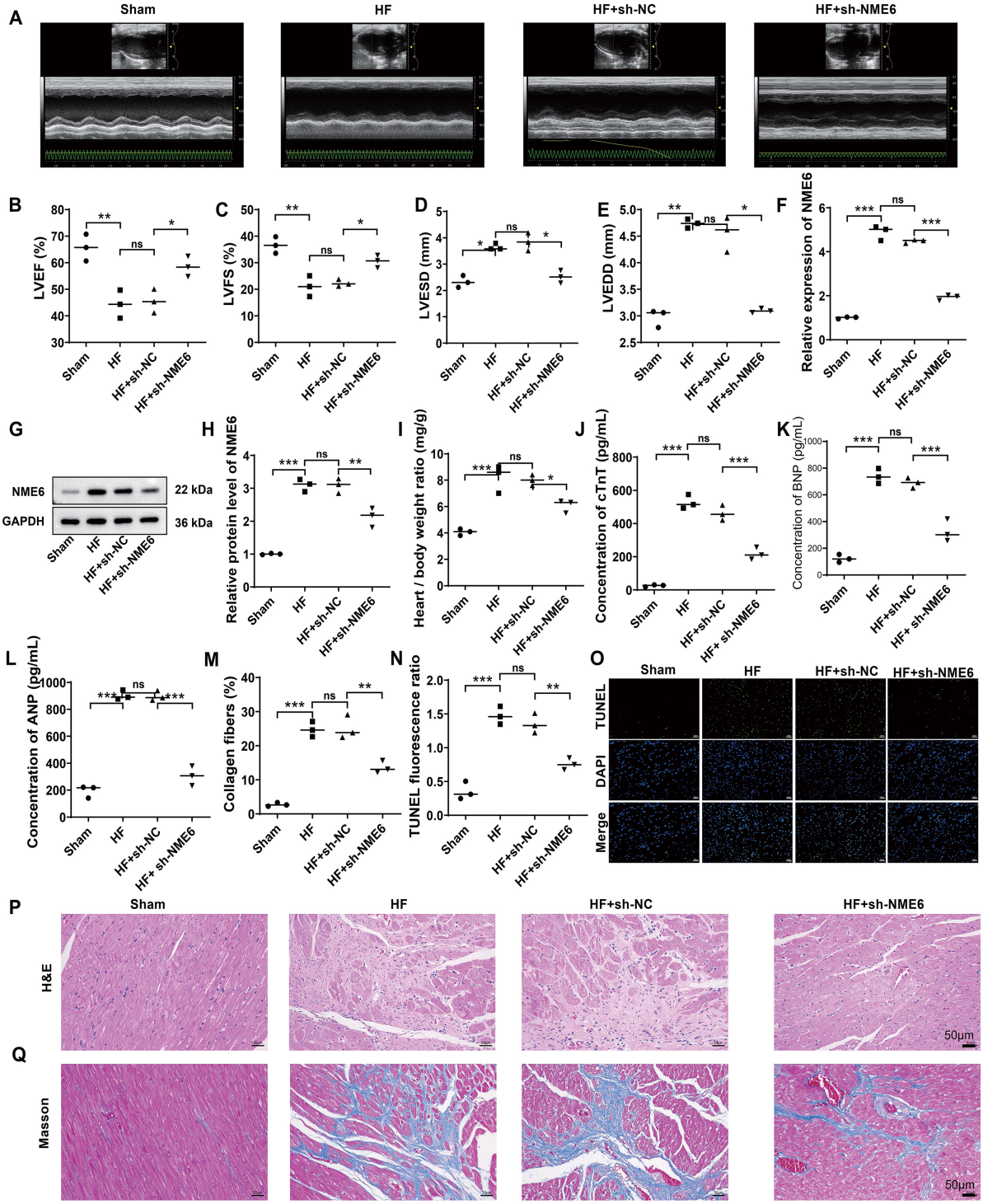

Fig. 4. ***NME6* knockdown alleviates HF in mice**. (A) Echocardiography was employed to assess HF status in mice, (B) Left ventricular ejection fraction (LVEF), (C) Left ventricular fractional shortening (LVFS), (D) Left ventricular end-diastolic diameter (LVEDD), (E) Left ventricular end-systolic diameter (LVESD). (F–H) Quantitative real-time polymerase chain reaction (qRT-PCR) and Western blot assays were used to measure the expression of *NME6* in the hearts of HF mice. (I) Heart weight to body weight ratio (HW/BW) in mice. (J) Serum cardiac troponin T (cTnT) levels in HF mice, (K) serum B-type natriuretic peptide (BNP) levels, (L) serum atrial natriuretic peptide (ANP) levels. (M) Statistical analysis of cardiac fibrosis in mice. (N,O) The effect of *NME6* knockdown on cardiomyocyte apoptosis in HF mice was assessed by terminal deoxynucleotidyl transferase dUTP nick end labeling (TUNEL) staining. Scale bar = 50 μm. (P) The effect of *NME6* knockdown on pathological changes in the hearts of HF mice was evaluated by hematoxylin and eosin (H&E) staining. Scale bar = 50 μm. (Q) The impact of *NME6* knockdown on cardiac fibrosis in HF mice was determined by Masson staining. Scale bar = 50 μm. ns: not significant, $^{*}p < 0.05$, $^{**}p < 0.01$, $^{***}p < 0.001$.

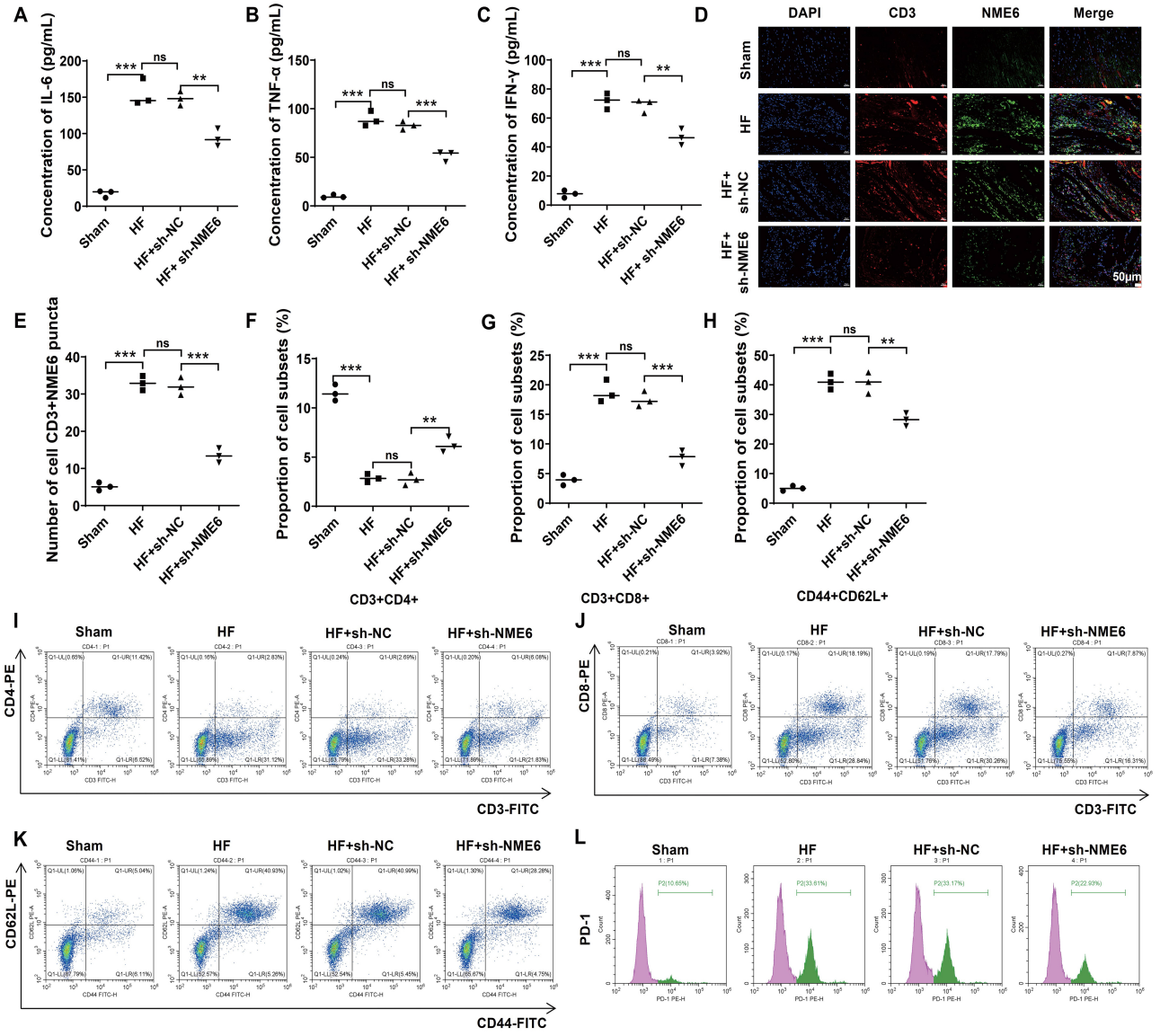

Fig. 5. NME6 knockdown alleviates inflammation in HF mice by altering the proportions of T cell subsets infiltrating the heart. (A) Serum IL-6 levels in mice, (B) serum TNF-α levels, (C) serum IFN-γ levels. (D,E) Immunofluorescence labeling was used to detect $CD3^+NME6^+$ cells in mouse heart tissue. Scale bar = 50 μm. (F–K) Flow cytometry was employed to measure the proportions of $CD3^+CD4^+$ cells, $CD3^+CD8^+$ cells, and $CD44^+CD62L^+$ cells. (L) Flow cytometry was used to determine the proportion of exhaustion markers ($PD\text{-}1^+$) cells. ns: not significant, $^{**}p < 0.01$, $^{***}p < 0.001$.

the connection between these mitochondrial genes and immunological dysregulation, a feature of the development of HF [11,13,16]. Dysregulated immune cell infiltration, particularly by macrophages, T cells, and neutrophils, exacerbates myocardial inflammation and fibrosis. Previously studies have reported that *NDUFS2* and *NME6* expression levels were strongly connected with the abundance of specific immune cell subsets [28,29]. *NDUFS2* showed favorable associations with memory B cells and $CD4^+$ naïve T cells, and negative correlations with naïve B cells and resting $CD4^+$ memory T cells. *NME6* was positively associated with $CD8^+$ T cells and eosinophils, but inversely connected with M1 macrophages and resting dendritic cells. These associations suggest that mitochondrial gene expression may influence immune cell composition and function in HF.

To further define NDUFS2 and NME6 cellular specificity, we analyzed scRNA-seq data from human HF cardiac tissue (GSE145154). UMAP clustering identified 15 major cell types, revealing that *NDUFS2* is expressed in multiple types of immune cells, while *NME6* is highly expressed in T cells and neutrophils. This observation provides a basis for functional studies, but it does not establish causality or the molecular pathways through which NME6 may act. To date, there have been few reports on the involvement of *NME6* in HF, highlighting the value of further exploring its role in the treatment of HF. Luo et al.

[28] found that elevated NME6 expression was linked to infiltrating immune cells, such as neutrophils. Additionally, Haglund et al. [30] reported that *NME6* may participate in inflammatory diseases by regulating T cells. Our study supports these findings, as *NME6* knockdown was found to upregulate the proportion of $CD4^+$ T cells, while reducing the proportions of $CD8^+$ T cells and $CD62L^+$ T cells. T cells have a vital part in both adaptive immunity and chronic inflammation, and they contribute to the development of HF [31]. Therefore, targeted modulation of particular T cell subsets may be a feasible treatment approach for HF. $CD4^+$ T cells and $CD8^+$ T cells are two major subsets of T cells, with $CD4^+$ T cells regulating the occurrence of immune responses [32]. However, when patients develop HF, the proportion of $CD4^+$ T cells usually decreases [33]. This may be related to factors such as increased left ventricular volume load and impaired myocardial contractile function in HF patients [34]. Furthermore, following myocardial infarction, CD8+ T cells, which are cytotoxic T lymphocytes, might be activated and destroy healthy heart cells [35]. Moreover, activated $CD8^+$ T cells can promote myocardial cell apoptosis, injury, and remodeling by secreting pro-inflammatory cytokines [36], thereby participating in the development of HF [35].

In conclusion, this integrative multi-omics study identified *NDUFS2* and *NME6* as mitochondrial genes of interest in HF, with potential involvement in both metabolic and immune regulation. Animal experiments further revealed that *NME6* can exacerbate the body's inflammatory response and promote the pathological progression of HF by influencing the relative distribution of $CD4^+$ T cells and $CD8^+$ T cells. These findings suggest that *NME6* may be a candidate biomarker and therapeutic target in the field of HF treatment.

5. Limitations

Several limitations of this study should be noted. First, the clinical cohort was limited by a relatively small sample size, an uneven distribution of patients across NYHA classes, and the absence of a healthy control group. These factors restrict the robustness of statistical analyses and limit the ability to draw definitive conclusions regarding the association between NME6 expression and HF severity. Therefore, the clinical findings should be interpreted as preliminary and exploratory. Moreover, whether the observed changes in T-cell subsets represent a direct immunoregulatory effect of NME6 or occur secondary to improvements in cardiac function requires further investigation. In addition, the cross-sectional nature of the clinical data precludes causal inference. Further experimental and clinical studies are warranted to elucidate the mechanistic roles of NME6 and to validate these findings in larger, well-balanced cohorts with appropriate control groups, as well as to explore targeted interventions that could modulate mitochondrial-immune crosstalk in HF.

6. Conclusion

Through integrative multi-omics analyses, this study identified *NDUFS2* and *NME6* as key mitochondrial genes with strong diagnostic potential in HF. Beyond their diagnostic value, these genes are intricately involved in mitochondrial function and cardiac-related pathways. Moreover, their expression is significantly correlated with immune cell infiltration in the heart tissue of HF patients, exhibiting distinct cell type specificity. Animal experiments suggest that NME6 may influence cardiac injury and modulate the proportions of $CD4^+$ and $CD8^+$ T cells in HF. These findings offer fresh insights into the molecular processes potentially driving HF.

Availability of Data and Materials

The datasets generated during and analyzed during the current study are available from the corresponding authors on reasonable request.

Author Contributions

Conception and design: RX, PL, SGW. Development of methodology: FY, JW, LY. Sample collection: XWQ, LY, XYQ. Analysis and interpretation of data: RX, PL, FY, SGW, YZ, JJK. Writing, review, and/or revision of the manuscript: PL, JJK, RX. All authors contributed to editorial changes in the manuscript. All authors read and approved the final manuscript. All authors have participated sufficiently in the work and agreed to be accountable for all aspects of the work.

Ethics Approval and Consent to Participate

The human study was approved by the Medical Ethics Committee of the First Affiliated Hospital of Anhui University of Traditional Chinese Medicine (Approval number: 2022AH-93) and conducted in accordance with the Declaration of Helsinki. Written informed consent was obtained from all participants. All animal experiments were approved by the Ethics Committee of the First Affiliated Hospital of Anhui University of Traditional Chinese Medicine (AZYFY-2024-1005) and performed in accordance with ARRIVE 2.0 guidelines and the Chinese national standard GB/T 35892-2018 (Laboratory animal -Guidelines for ethical review of animal welfare).

Acknowledgment

Not applicable.

Funding

This study was supported by the National Key R&D Program of China (2022YFC3500502), Anhui Provincial Scientific Research Planning Project (2023AH050796) and University talent support program (2023rcyb002).

Conflicts of Interest

The authors declare no conflicts of interest.

Declaration of AI and AI-Assisted Technologies in the Writing Process

During the preparation of this work, the authors used ChatGPT-5.1 to check spelling and grammar. After using this tool, the authors thoroughly reviewed and edited the content as needed and take full responsibility for the integrity of the publication.

Supplementary Material

Supplementary material associated with this article can be found, in the online version, at https://doi.org/10.31083/FBL48958.

References

[1] Ranek M, Berthiaume J, Kirk J, Lyon R, Sheikh F, Jensen B, et al. Pathophysiology of heart failure and an overview of therapies. In Buja LM, Butany J (eds.) Cardiovascular Pathology (pp. 149–221). Academic Press: Cambridge, Massachusetts, USA. 2022. https://doi.org/10.1016/B978-0-12-822224-9.00025-6

[2] Tran P, Maddock H, Banerjee P. Myocardial Fatigue: a Mechano-energetic Concept in Heart Failure. Current Cardiology Reports. 2022; 24: 711–730. https://doi.org/10.1007/s11886-022-01689-2

[3] Martins LK, Polezer CN, Mouzully MAC, Silva LAGPd, Carvalho ARdS, et al. Symptom experience in people with heart failure in the context of Symptom Management Theory. Escola Anna Nery. 2025; 28: e20240022. https://doi.org/10.1590/2177-9465-EAN-2024-0022en

[4] Jering K, Claggett B, Redfield MM, Shah SJ, Anand IS, Martinez F, et al. Burden of Heart Failure Signs and Symptoms, Prognosis, and Response to Therapy: The PARAGON-HF Trial. JACC. Heart Failure. 2021; 9: 386–397. https://doi.org/10.1016/j.jchf.2021.01.011

[5] Naser A, Güvenç TS, Isgandarov K, Ekmekçi A, Gündüz S, Çetin Güvenç R, et al. Lack of right ventricular hypertrophy is associated with right heart failure in patients with left ventricular failure. Heart and Vessels. 2022; 37: 1728–1739. https://doi.org/10.1007/s00380-022-02075-2

[6] Dini FL, Pugliese NR, Ameri P, Attanasio U, Badagliacca R, Correale M, et al. Right ventricular failure in left heart disease: from pathophysiology to clinical manifestations and prognosis. Heart Failure Reviews. 2023; 28: 757–766. https://doi.org/10.1007/s10741-022-10282-2

[7] Rosenkranz S, Howard LS, Gomberg-Maitland M, Hoeper MM. Systemic Consequences of Pulmonary Hypertension and Right-Sided Heart Failure. Circulation. 2020; 141: 678–693. https://doi.org/10.1161/CIRCULATIONAHA.116.022362

[8] Andreadou I, Ghigo A, Nikolaou PE, Swirski FK, Thackeray JT, Heusch G, et al. Immunometabolism in heart failure. Nature Reviews. Cardiology. 2025; 22: 751–772. https://doi.org/10.1038/s41569-025-01165-8

[9] Müller M, Bischof C, Kapries T, Wollnitza S, Liechty C, Geißen S, et al. Right Heart Failure in Mice Upon Pressure Overload Is Promoted by Mitochondrial Oxidative Stress. JACC. Basic to Translational Science. 2022; 7: 658–677. https://doi.org/10.1016/j.jacbts.2022.02.018

[10] Bisaccia G, Ricci F, Gallina S, Di Baldassarre A, Ghinassi B. Mitochondrial Dysfunction and Heart Disease: Critical Appraisal of an Overlooked Association. International Journal of Molecular Sciences. 2021; 22: 614. https://doi.org/10.3390/ijms22020614

[11] Lopaschuk GD, Karwi QG, Tian R, Wende AR, Abel ED. Cardiac Energy Metabolism in Heart Failure. Circulation Research. 2021; 128: 1487–1513. https://doi.org/10.1161/CIRCRESAHA.121.318241

[12] Bhullar SK, Dhalla NS. Status of Mitochondrial Oxidative Phosphorylation during the Development of Heart Failure. Antioxidants (Basel, Switzerland). 2023; 12: 1941. https://doi.org/10.3390/antiox12111941

[13] Hinton A, Jr, Claypool SM, Neikirk K, Senoo N, Wanjalla CN, Kirabo A, et al. Mitochondrial Structure and Function in Human Heart Failure. Circulation Research. 2024; 135: 372–396. https://doi.org/10.1161/CIRCRESAHA.124.323800

[14] Kumar V, Santhosh Kumar TR, Kartha CC. Mitochondrial membrane transporters and metabolic switch in heart failure. Heart Failure Reviews. 2019; 24: 255–267. https://doi.org/10.1007/s10741-018-9756-2

[15] Cabello-Rivera D, Sarmiento-Soto H, López-Barneo J, Muñoz-Cabello AM. Mitochondrial Complex I Function Is Essential for Neural Stem/Progenitor Cells Proliferation and Differentiation. Frontiers in Neuroscience. 2019; 13: 664. https://doi.org/10.3389/fnins.2019.00664

[16] Marin SE, Mesterman R, Robinson B, Rodenburg RJ, Smeitink J, Tarnopolsky MA. Leigh syndrome associated with mitochondrial complex I deficiency due to novel mutations In NDUFV1 and NDUFS2. Gene. 2013; 516: 162–167. https://doi.org/10.1016/j.gene.2012.12.024

[17] Han S, Lee M, Shin Y, Giovanni R, Chakrabarty RP, Herrerias MM, et al. Mitochondrial integrated stress response controls lung epithelial cell fate. Nature. 2023; 620: 890–897. https://doi.org/10.1038/s41586-023-06423-8

[18] Du H, Zhao Y, Wen J, Dai B, Hu G, Zhou Y, et al. LncRNA DCRT Protects Against Dilated Cardiomyopathy by Preventing NDUFS2 Alternative Splicing by Binding to PTBP1. Circulation. 2024; 150: 1030–1049. https://doi.org/10.1161/CIRCULATIONAHA.123.067861

[19] Proust B, Radić M, Vidaček NŠ, Cottet C, Attia S, Lamarche F, et al. NME6 is a phosphotransfer-inactive, monomeric NME/NDPK family member and functions in complexes at the interface of mitochondrial inner membrane and matrix. Cell & Bioscience. 2021; 11: 195. https://doi.org/10.1186/s13578-021-00707-0

[20] Grotehans N, McGarry L, Nolte H, Xavier V, Kroker M, Narbona-Pérez ÁJ, et al. Ribonucleotide synthesis by NME6 fuels mitochondrial gene expression. The EMBO Journal. 2023; 42: e113256. https://doi.org/10.15252/embj.2022113256

[21] Schlattner U. The Complex Functions of the NME Family-A Matter of Location and Molecular Activity. International Journal of Molecular Sciences. 2021; 22: 13083. https://doi.org/10.3390/ijms222313083

[22] Liberzon A, Subramanian A, Pinchback R, Thorvaldsdóttir H, Tamayo P, Mesirov JP. Molecular signatures database (MSigDB) 3.0. Bioinformatics (Oxford, England). 2011; 27: 1739–1740. https://doi.org/10.1093/bioinformatics/btr260

[23] He Y, Huang W, Zhang C, Chen L, Xu R, Li N, et al. Energy metabolism disorders and potential therapeutic drugs in heart failure. Acta Pharmaceutica Sinica. B. 2021; 11: 1098–1116. https://doi.org/10.1016/j.apsb.2020.10.007

[24] Ye H, Lin J, Zhang H, Wang J, Fu Y, Zeng Z, et al. Nuclear receptor 4A1 Regulates Mitochondrial Homeostasis in Cardiac Post-Ischemic Injury by Controlling Mitochondrial Fission 1 Protein-Mediated Fragmentation and Parkin-Dependent Mitophagy. International Journal of Biological Sciences. 2025; 21: 400–414. https://doi.org/10.7150/ijbs.104680

[25] Barth AS, Kumordzie A, Tomaselli GF. Orchestrated regulation

of energy supply and energy expenditure: Transcriptional coexpression of metabolism, ion homeostasis, and sarcomeric genes in mammalian myocardium. Heart Rhythm. 2016; 13: 1131–1139. https://doi.org/10.1016/j.hrthm.2016.01.009

[26] Wolin MS, Alruwaili N, Kandhi S. Studies on Hypoxic Pulmonary Vasoconstriction Detect a Novel Role for the Mitochondrial Complex I Subunit Ndufs2 in Controlling Peroxide Generation for Oxygen-Sensing. Circulation Research. 2019; 124: 1683–1685. https://doi.org/10.1161/CIRCRESAHA.119.315137

[27] Dunham-Snary KJ, Wu D, Potus F, Mewburn JD, Charles RL, Eaton P, et al. Ndufs2, a Core Subunit of Mitochondrial Complex I, Is Essential for Acute Oxygen-Sensing and Hypoxic Pulmonary Vasoconstriction. Circulation Research. 2019; 12: 1727–1746. https://doi.org/10.1161/CIRCRESAHA.118.314284

[28] Luo L, Li Y, Zhang L, Yang L. NME6 as a potential biomarker and therapeutic target involved in immune infiltration for lung adenocarcinoma. Technology and Health Care : Official Journal of the European Society for Engineering and Medicine. 2024; 32: 2277–2291. https://doi.org/10.3233/THC-231058

[29] Zou X, Huang Q, Kang T, Shen S, Cao C, Wu J. An integrated investigation of mitochondrial genes in COPD reveals the causal effect of NDUFS2 by regulating pulmonary macrophages. Biology Direct. 2025; 20: 4. https://doi.org/10.1186/s13062-025-00593-3

[30] Haglund S, Almer S, Peterson C, Söderman J. Gene expression and thiopurine metabolite profiling in inflammatory bowel disease - novel clues to drug targets and disease mechanisms? PloS One. 2013; 8: e56989. https://doi.org/10.1371/journal.pone.0056989

[31] Li J, Liu L, Luo Q, Zhou W, Zhu Y, Jiang W. Exploring the causal relationship between immune cell and all-cause heart failure: a Mendelian randomization study. Frontiers in Cardiovascular Medicine. 2024; 11: 1363200. https://doi.org/10.3389/fcvm.2024.1363200

[32] Lu X, Xv Y, Hu W, Sun B, Hu H. Targeting CD4+ T cells through gut microbiota: therapeutic potential of traditional Chinese medicine in inflammatory bowel disease. Frontiers in Cellular and Infection Microbiology. 2025; 15: 1557331. https://doi.org/10.3389/fcimb.2025.1557331

[33] Tang TT, Zhu ZF, Wang J, Zhang WC, Tu X, Xiao H, et al. Impaired thymic export and apoptosis contribute to regulatory T-cell defects in patients with chronic heart failure. PloS One. 2011; 6: e24272. https://doi.org/10.1371/journal.pone.0024272

[34] Ovchinnikov A, Filatova A, Potekhina A, Arefieva T, Gvozdeva A, Ageev F, et al. Blood Immune Cell Alterations in Patients with Hypertensive Left Ventricular Hypertrophy and Heart Failure with Preserved Ejection Fraction. Journal of Cardiovascular Development and Disease. 2023; 10: 310. https://doi.org/10.3390/jcdd10070310

[35] Zhang L, Wang Z, Wang D, Zhu J, Wang Y. $CD8^{+}CD28^{+}$ T cells might mediate injury of cardiomyocytes in acute myocardial infarction. Molecular Immunology. 2018; 101: 74–79. https://doi.org/10.1016/j.molimm.2018.05.015

[36] de Carvalho GC, Domingues R, de Sousa Nogueira MA, Calvielli Castelo Branco AC, Gomes Manfrere KC, Pereira NV, et al. Up-regulation of Proinflammatory Genes and Cytokines Induced by S100A8 in CD8+ T Cells in Lichen Planus. Acta Dermato-venereologica. 2016; 96: 485–489. https://doi.org/10.2340/00015555-2306